

# G<sup>2</sup>V<sup>2</sup>former: Graph Guided Video Vision Transformer for Face Anti-Spoofing

Jingyi Yang<sup>1</sup>, Zitong Yu<sup>2\*</sup>, Jia He<sup>3</sup>, Xiuming Ni<sup>3</sup>, Hui Li<sup>1†</sup>

<sup>1</sup> Dept. EEIS, University of Science and Technology of China

The CAS Key Laboratory of Wireless-Optical Communications

<sup>2</sup> School of Computing and Information Technology, Great Bay University

<sup>3</sup> Anhui Tsinglink Information Technology Co.,Ltd.

yangjingyi@mail.ustc.edu.cn yuzitong@gbu.edu.cn {hejia, nixm}@tsinglink.com mythlee@ustc.edu.cn

## Abstract

In videos containing spoofed faces, we may uncover the spoofing evidence based on either photometric or dynamic abnormality, even a combination of both. Prevailing face anti-spoofing (FAS) approaches generally concentrate on the single-frame scenario, however, purely photometric-driven methods overlook the dynamic spoofing clues that may be exposed over time. This may lead FAS systems to conclude incorrect judgments, especially in cases where it is easily distinguishable in terms of dynamics but challenging to discern in terms of photometrics. To this end, we propose the Graph Guided Video Vision Transformer (G<sup>2</sup>V<sup>2</sup>former), which combines faces with facial landmarks for photometric and dynamic feature fusion. We factorize the attention into space and time, and fuse them via a spatiotemporal block. Specifically, we design a novel temporal attention called Kronecker temporal attention, which has a wider receptive field, and is beneficial for capturing dynamic information. Moreover, we leverage the low-semantic motion of facial landmarks to guide the high-semantic change of facial expressions based on the motivation that regions containing landmarks may reveal more dynamic clues. Extensive experiments on nine benchmark datasets demonstrate that our method achieves superior performance under various scenarios. The codes will be released soon.

## Introduction

Face recognition (FR), as the most remarkable and successful biometric recognition technology, has been widely applied in different scenarios such as access control and mobile electronic payments. Despite its success, FR systems are vulnerable to various presentation attacks, including printed photos, video replay, 3D masks, etc. Fortunately, face anti-spoofing (FAS) techniques have been proven to play a crucial role in enhancing the security of FR systems. Consequently, this topic has gradually emerged as a recent research hotspot.

\*Equal Corresponding Author. This work was supported by Guangdong Basic and Applied Basic Research Foundation (Grant No. 2023A1515140037).

†Corresponding Author. This work was supported by the National Science Foundation of China, under Grant No. 62171425

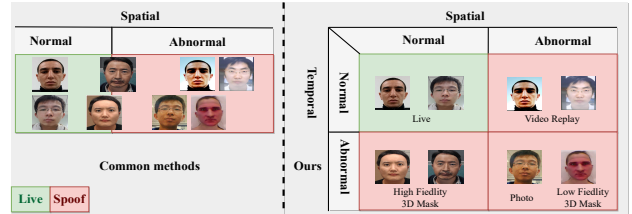


Figure 1: Most common methods in FAS focus on frame-level spoofing representation. In contrast, our method aims to fuse photometric and dynamic spoofing clues. When the testing sample shows abnormalities in any dimension (space or time), it should be detected as a spoof.

Most previous research focuses on frame-level anti-spoofing, including but not limited to extracting hand-crafted texture (Boulkenafet, Komulainen, and Hadid 2015; Patel, Han, and Jain 2016b; Yang et al. 2013), and deeply learned representations (Li et al. 2016a; Yu et al. 2020b), adopting domain generalization (Shao et al. 2019; Jia et al. 2020; Chen et al. 2021; Liu et al. 2021c; Wang et al. 2022c; Zhou et al. 2023; Sun et al. 2023; Yang et al. 2024), and domain adaptation (Wang et al. 2020a, 2021a) techniques, attempting meta-learning paradigms (Shao, Lan, and Yuen 2020; Wang et al. 2021a; Liu et al. 2021c), and so on. Generally speaking, their common goal is to capture the photometric distinction between live and spoof faces, hoping that it is universal. Despite their significant success in FAS tasks, they overlook the possibility that spoof clues may be exposed over time. A pure photometric-driven algorithm has not fully mined the spoofing information contained in videos and might be insufficient to represent the intrinsic gap between the live and spoof, as shown in the left of Figure 1.

There are already several efforts to explore spatiotemporal anti-spoofing features at the video level. Some research exploits the models comprised of CNN-LSTM/GRU (Liu, Jourabloo, and Liu 2018; Saha et al. 2020; Wang et al. 2020b; Yang et al. 2019), 3D-CNNs (Wang et al. 2021b; Xu et al. 2021), or transformers (Ming et al. 2022; Khan and Dai 2021; Wang et al. 2022b; Khan and Dai 2021; Wang et al. 2022b). Recently, GAIN (Chang et al. 2023) proposes combining the skeleton-based action recognition

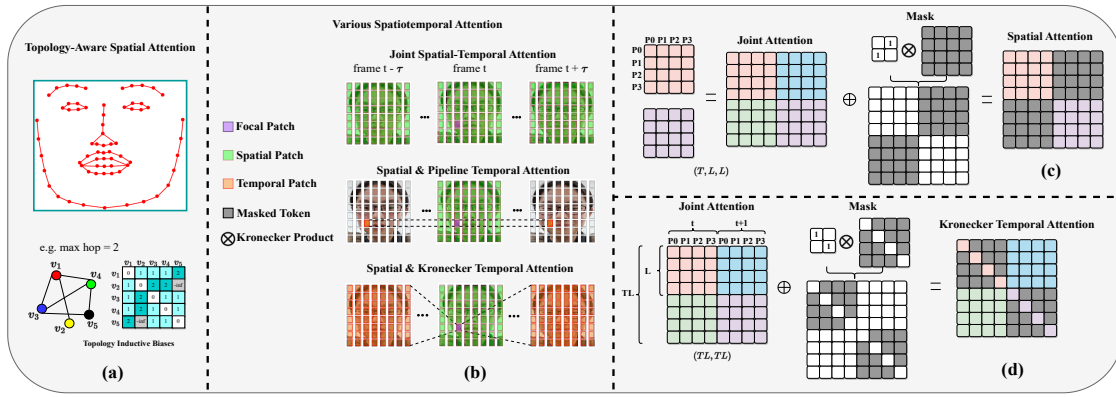


Figure 2: (a) The topology-aware spatial attention. Connections between two nodes will be blocked (masked in attention matrix) if they are too far apart in the topology. (b) Various visual spatiotemporal attention. (c) Common spatial attention can be seen as applying a mask to joint attention. (d) Kronecker temporal attention can also be obtained by employing a tailored mask to joint attention. Spatial attention and Kronecker temporal attention exhibit spatiotemporal complementarity.

with photometric-based face anti-spoofing. They utilize ST-GCN (Yan, Xiong, and Lin 2018) to capture the motion information contained in facial landmarks and integrate it with existing photometric-based FAS frameworks showing an extraordinary performance. However, landmarks are only three-dimensional coordinates (low-semantic), may not be enough to carry complex dynamic information like pixel motion.

Aiming to fully exploit spoofing clues in both spatial and temporal dimensions, we propose a transformer-based architecture that both images and landmarks as inputs to integrate photometric feature with dynamic information. We factorize the attention to spatial and temporal dimensions, the spatial attention in vision aggregates the photometric feature and topology-aware spatial attention serves for the perception of facial contours through landmarks, as shown in Figure 2 (a) and (b). Our proposed Kronecker temporal attention exhibits a wider receptive field, and is conducive for global dynamic information capture, as illustrated in Figure 2 (b) and (d). We extract rough facial motion through temporal attention of landmarks and then guiding the temporal attention of vision branch focuses on patches that are more likely to occur pixel motion. Our main contributions are three-folds:

- We propose a novel architecture Graph Guided Video Vision Transformer ( $G^2V^2$ former) to fuse the spatial and temporal information from video and landmarks for face anti-spoofing tasks as depicted in the right of Figure 1, achieving remarkable generalization capability.
- We design a novel Kronecker temporal attention (KTA) which is more conducive to capturing the patch or node relationship of different timestamps and is beneficial to capturing comprehensive temporal clues.
- We propose the graph-guided vision temporal attention which leverage temporal attention of landmarks motion to guide the capture of the higher-semantic pixel motion.

## Related Work

**Mining Temporal Clues for Face Anti-Spoofing.** A series of face anti-spoofing methods (Li et al. 2016b; Liu, Jourabloo, and Liu 2018; Liu, Lan, and Yuen 2018; Yu et al. 2021) attempt to utilize temporal information in a video clip, especially the representative biological activity signal, Remote Photoplethysmography (rPPG) signal. Because rPPG signals are only detectable from live, not spoof, individuals. However, they overly rely on the credibility and robustness of the extracted rPPG signals and requires a sufficiently long video. Some approaches are based on the changes in facial expressions such as eyes blinking (Patel, Han, and Jain 2016a), movements of mouth and lip (Kollreider et al. 2007; Shao, Lan, and Yuen 2017). Other methods, like (Liu, Jourabloo, and Liu 2018; Saha et al. 2020; Wang et al. 2020b; Yang et al. 2019; Wang et al. 2021b; Xu et al. 2021), capture temporal correlation by designing unique network architectures. While other studies (Ming et al. 2022; Khan and Dai 2021; Wang et al. 2022b) based on transformers have been explored for FAS task. For example, Khan et al. (Khan and Dai 2021) propose a video transformer with incremental learning for detecting deepfake videos, and TTN (Wang et al. 2022b) employs a temporal transformer network and a temporal depth difference loss to learn multi-granularity temporal characteristics for FAS. Recently, GAIN (Chang et al. 2023) adopted ST-GCN (Yan, Xiong, and Lin 2018) to extract the deeply learned spatial-temporal features from facial landmarks and extracted photometric features by existing photometric-based methods.

**Spatiotemporal Representation Fusion.** Except for the excellent modeling ability for long-range dependencies, the self-attention mechanism is more flexible, beneficial, and suitable than 3D convolution when dealing with video and conducting spatiotemporal fusion. Several recent attempts have been made to extend ViT (Dosovitskiy et al. 2020) to the video domain (Bertasius, Wang, and Torresani 2021; Arnab et al. 2021; Neimark et al. 2021; Guo, Guo, and Lu 2021; Liu et al. 2022). They introduce various calculation

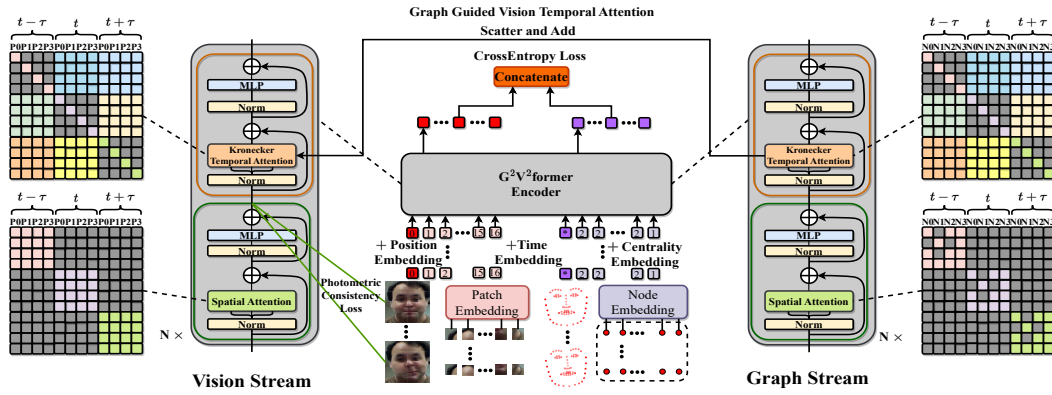


Figure 3: The architecture of graph guided video vision transformer. It requires inputting a facial video clip into the vision stream and the corresponding facial landmarks into the graph stream. The visual spatial attention is guided by photometric consistency loss, while the visual temporal attention is guided by graphic temporal attention via scatter and add operation. We concatenate the head token of both stream for classification, and optimized it through cross-entropy loss.

forms of spatiotemporal attention which can be mainly categorized into two common types, i.e., joint and divided as shown in Figure 2. Furthermore, the pioneering work of MAE (He et al. 2022) proved that using the paradigm of predicting masked content for visual tasks’ self-supervised learning also yields remarkable advantages. Just like ViT is easy to expand into the video domain. The MAE has also launched a video version (Feichtenhofer et al. 2022; Tong et al. 2022). Typically, they need a higher masking ratio because videos have greater redundancy. Compared to images, videos have more masking strategies, (Feichtenhofer et al. 2022) explores four common masking strategies.

## Methodology

The Graph Guided Video Vision Transformer ( $G^2V^2$ former) is a two-stream architecture designed to fuse both static and dynamic spoofing clues from faces and landmarks. We adopt a cascaded form of spatiotemporal attention. The architecture of  $G^2V^2$ former is shown in Figure 3. A spatiotemporal block (STB) of vision stream or graph stream consists of a spatial and a temporal attention module, used for spatiotemporal feature fusion. Vision or graph stream are composed of multiple STB stacked together. Our training process is divided into two stages. During the first stage, we implement the MAE’s pre-training paradigm. Note that the pre-training for the vision stream and graph stream is conducted independently. We fine-tune the  $G^2V^2$ former and utilize the graph stream to guide the vision stream in the second stage.

We set the masking ratio at 90% both in the vision stream and graph stream during pre-training. Please note that we employ a 90% masking ratio for each frame, ensuring consistency in the masking ratio across all frames, nonetheless, the positions of the masked areas may differ. We hope that our spatial and temporal attention modules can be equally trained. Absolute positional and temporal embedding was added. The original landmarks are three-dimensional coordinate points, in order to enable the network to better sense high-frequency changes in coordinates, we used sine-cosine

positional encoding derived from (Mildenhall et al. 2021), where  $L$  is the number of frequencies:

$$\gamma(x) = (\sin(2^0 \pi x), \cos(2^0 \pi x), \dots, \sin(2^{L-1} \pi x), \cos(2^{L-1} \pi x)) \quad (1)$$

In the fine-tuning stage, we concatenate the class tokens of vision stream and hyper-node tokens of graph stream. They are used for classification.

## Photometric Consistency in Spatial Attention

First, we implement patch embedding like ViT (Dosovitskiy et al. 2020), splitting each image into patches. Then flatten the patches and conduct standard self-attention calculations. Spatial Attention (SA):

$$Q_s = x_{(l \times d)} W_Q, K_s = x_{(l \times d)} W_K, V_s = x_{(l \times d)} W_V, \quad (2)$$

$$Z_s = \text{Softmax}(Q_s K_s^T / \sqrt{d_k} + B) V_s \quad (3)$$

Spatial Attention Module:

$$Z_s = \text{SA}(\text{LN}(X)) + X, \quad (4)$$

$$O_s = \text{MLP}(\text{LN}(Z_s)) + Z_s, \quad (5)$$

where  $x_{(l \times d)}$  denotes the embedding of patches,  $l$  represents the number of tokens, and  $d$  ( $d_k$ ) is the token dimension.  $Q$ ,  $K$ ,  $V$ , which are the query matrix, key matrix, and value matrix.  $B$  is the relative position attention bias (Liu et al. 2021e). LN is the layer normalization, and MLP is a two-layer non-linear fully connected neural network.

In order to enhance the spatial attention to photometric abnormality, we propose photometric consistency loss (PCL) to increase the similarity between different frames in the same video as follow:

$$L_{PCL} = \begin{cases} -\frac{1}{BT} \sum_i^{BT} \sum_j^{BT} \frac{\exp(s_{i,j}/\tau)}{\sum_{k \neq i}^{BT} \exp(s_{i,k}/\tau)}, & y = 1 \\ -\frac{1}{BT} \sum_i^{BT} \sum_j^{BT} \mathbb{I}(\lfloor \frac{i}{T} \rfloor = \lfloor \frac{j}{T} \rfloor) \frac{\exp(s_{i,j}/\tau)}{\sum_{k \neq i}^{BT} \exp(s_{i,k}/\tau)}, & y = 0 \end{cases} \quad (6)$$

where  $\tau$  is a temperature parameter,  $y$  represents the liveness label (1 is live, 0 is spoof).  $s_{i,j}$  is the cosine similarity between  $i$ -th class token and  $j$ -th class token.  $B$  denotes the

batch size,  $T$  denotes the number of frames.  $\lfloor \frac{i}{T} \rfloor$  represents round down.

Notably, we treat live and spoof samples asymmetrically, bringing all live frames from different videos closer in the representation space, while only gathering the spoof frames from the same video closer in the representation space. As the photometric characteristics between live samples exhibit a high degree of homogeneity, in contrast, spoof samples exhibit a high degree of heterogeneity.

### Topology-aware Spatial Attention

We consider the facial landmarks extracted from the video as spatiotemporal graph data. However, transformers inherently have a global receptive field, enabling information aggregation between any two tokens. This innate property may lead to ambiguity regarding positional information. This phenomenon is particularly pronounced in graph-structured data, which lacks a sequential structure and 2D inductive bias. We draw inspiration from Graphormer (Ying et al. 2021) and propose topology-aware spatial attention for graph learning. For any undirected graph, the adjacency matrix can represent the topology relationships among nodes. Fortunately, the intrinsic topology capacity of the adjacency matrix can also be achieved by an attention mask that can reflect the topology. Specifically, when there is no connection between two nodes, the attention weight ( $QK^T(i, j)$ ) between the two nodes will be set to negative infinity, signifying a lack of direct information interaction. We define a function  $\phi_h(v_i, v_j)$  to express the adjacency relationship between two nodes, if node  $v_i$  cannot reach node  $v_j$  within a maximum of  $h$  hops, it is considered that there is no connection between  $v_i$  and  $v_j$ . Otherwise, the shortest number of hops between  $v_i$  and  $v_j$  serves as the relative distance between them:

$$\phi_h(v_i, v_j) = \begin{cases} \text{Embed}(\text{hop}_{\min}(v_i, v_j)), & \text{hop}_{\min}(v_i, v_j) \leq h \\ -\text{inf}, & \text{otherwise} \end{cases} \quad (7)$$

$$B_{\text{graph}}(i, j) = \phi_h(v_i, v_j) \quad (8)$$

The output of function  $\phi_h(v_i, v_j)$  is a learnable real value, and the  $\text{hop}_{\min}(v_i, v_j)$  represents the minimum hop from  $v_i$  to  $v_j$ , returning an index that corresponds to the learnable real value. The schematic diagram, is shown on the left of Figure 2.

Simultaneously, each node, apart from having different coordinate values, holds varying importance within the entire graph, i.e., a measure known as node centrality. Thus we use the centrality encoding, which is associated with degree, we add it to the node embedding:

$$h_{v_i} = \text{NodeEmbed}(\gamma(x_{v_i})) + \text{DegreeEmbed}(v_i), \quad (9)$$

where  $x_{v_i}$  is the original coordinates of landmarks,  $h_{v_i}$  denotes the feature embedding of nodes with degree embedding.

### Kronecker Temporal Attention

The pipeline temporal attention cannot ensure interested objects always appear in patches at the same spatial location, thereby limiting the scope of capturing dynamic clues,

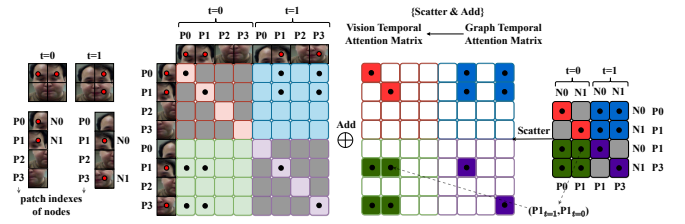


Figure 4: Graph-guided vision temporal attention. First, performing a scatter operation to align the shape of the graphic temporal attention matrix with that of the visual temporal attention matrix, and then adding them together.

due this form of temporal receptive field is constrain within a time pipeline, we refer to it as pipeline temporal attention. This may lead to the model deviating in their understanding of information, especially in tasks such as face anti-spoofing. To address these drawbacks, we introduce the Kronecker temporal attention. Specifically, a patch at timestamp  $t$  can interact with all other patches, excluding those sharing the same timestamp  $t$ . It will increase the search range (wider temporal receptive field) of each patch in temporal dimension and can adaptively capture favorable information. Compared to the combination of pipeline temporal attention and spatial attention, the combination of Kronecker temporal attention and spatial attention has better spatiotemporal complementarity. This attention mode can be achieved through the joint attention employed a mask. The trick for obtaining the temporal attention mask is using the Kronecker product. Hence, we term it Kronecker temporal attention. An illustration is presented in Figure 2.

Kronecker Temporal Attention (KTA):

$$Q_t = x_{(tl \times d)} W_Q, K_t = x_{(tl \times d)} W_K, V_t = x_{(tl \times d)} W_V, \quad (10)$$

$$M_{(tl \times tl)} = [I_{(t \times t)} \otimes (J_{(m \times m)} - I_{(m \times m)})]_{1===-\text{inf}}, \quad (11)$$

$$Z_t = \text{Softmax}(Q_t K_t^T / \sqrt{d_k} + M) V_t \quad (12)$$

Kronecker Temporal Attention Module:

$$Z_t = \text{KTA}(\text{LN}(X)) + X, \quad (13)$$

$$O_t = \text{MLP}(\text{LN}(Z_t)) + Z_t, \quad (14)$$

where  $x_{(tl \times d)}$  denotes the embedding of patches or nodes from  $t$  frames,  $tl$  represents the number of tokens from  $t$  frames and  $d$  ( $d_k$ ) is the token dimension.  $I$  represents an identity matrix,  $J$  is the all-ones matrix,  $[ ]_{1===-\text{inf}}$  means replacing ones in the matrix with negative infinity,  $M$  is the temporal attention mask.

### Graph Guided Vision Temporal Attention

The video datasets from face anti-spoofing exhibit significant differences from general video datasets attributed to the similarity in facial structures (high content homogeneity) and the subtle, inconspicuous motion of faces in videos. Although the Kronecker temporal attention can compensate for the shortcomings of limited temporal receptive field, focusing on a wider scope to search for dynamic clues, but it may struggle to quickly locate key motion areas. Hence, we



Table 1: Comparison to state-of-the-art FAS method under the LOO setting. The bold numbers indicate the SOTA, star marks (\*) the video-based methods. Others are single-frame-level methods.

Method	O&C&I to M		O&M&I to C		O&C&M to I		I&C&M to O	
	HTER(%)	AUC(%)	HTER(%)	AUC(%)	HTER(%)	AUC(%)	HTER(%)	AUC(%)
MMD-AAE (Li et al. 2018)	27.08	83.19	44.59	58.29	31.58	75.18	40.98	63.08
MADDG (Shao et al. 2019)	17.69	88.06	24.50	84.51	22.19	84.99	27.98	80.02
NAS-FAS (Yu et al. 2020a)	19.53	88.63	16.54	90.18	14.51	93.84	13.80	93.43
RFM (Shao, Lan, and Yuen 2020)	13.89	93.98	20.27	88.16	17.30	90.48	16.45	91.16
SSDG (Jia et al. 2020)	7.38	97.17	10.44	95.94	11.71	96.59	15.61	91.54
D <sup>2</sup> AM (Chen et al. 2021)	12.70	95.66	20.98	85.58	15.43	91.22	15.27	90.87
DRDG (Liu et al. 2021d)	12.43	95.81	19.05	88.79	15.56	91.79	15.63	91.75
ANRL (Liu et al. 2021c)	10.83	96.75	17.83	89.26	16.03	91.04	15.67	91.90
SSAN (Wang et al. 2022c)	6.67	98.75	10.00	96.67	8.88	96.79	13.72	93.63
PatchNet (Wang et al. 2022a)	7.10	98.46	11.33	94.58	13.40	95.67	11.82	95.07
IADG (Zhou et al. 2023)	5.41	98.19	8.70	96.44	10.62	94.50	8.86	97.14
SA-FAS (Sun et al. 2023)	5.95	96.55	8.78	95.37	6.58	97.54	10.00	96.23
UDG-FAS (Liu et al. 2023)	5.95	98.47	9.82	96.76	5.86	98.62	10.97	95.36
TTDG (Zhou et al. 2024)	7.91	96.83	8.14	96.49	6.50	97.98	10.00	95.70
GAC-FAS (Le and Woo 2024)	5.00	97.56	8.20	95.16	<b>4.29</b>	98.87	8.60	<b>97.16</b>
Auxiliary (Liu, Jourabloo, and Liu 2018)*	22.72	85.88	33.52	73.15	29.14	71.69	30.17	77.61
CCDD(Saha et al. 2020)*	15.42	91.13	17.41	90.12	15.87	91.72	14.72	93.08
GAIN (Chang et al. 2023)*	4.05	98.92	8.52	96.02	8.50	97.27	12.50	95.12
<b>G<sup>2</sup>V<sup>2</sup>former*</b>	<b>3.72</b>	<b>99.24</b>	<b>5.59</b>	<b>97.64</b>	5.42	<b>98.95</b>	<b>8.21</b>	97.04

Table 2: Evaluation on cross-domain protocols among CASIA-SURF (S), CASIA-CeFA (C), WMCA (W)

Method	CS → W		SW → C		CW → S	
	HTER ↓ (%)	AUC ↑ (%)	HTER ↓ (%)	AUC ↑ (%)	HTER ↓ (%)	AUC ↑ (%)
0-shot						
SSDG (Jia et al. 2020)	12.64	94.35	12.25	94.78	27.08	80.05
VIT (Huang et al. 2022)	7.98	97.97	11.13	95.46	13.35	94.13
<b>G<sup>2</sup>V<sup>2</sup>former</b>	<b>6.21</b>	<b>98.56</b>	<b>10.03</b>	<b>95.42</b>	<b>12.66</b>	<b>94.17</b>
5-shot						
SSDG (Jia et al. 2020)	5.08	99.02	6.72	98.11	18.88	88.25
VIT (Huang et al. 2022)	4.30	99.16	7.69	97.66	12.26	94.40
VITAF (Huang et al. 2022)	4.51	99.44	7.21	97.69	11.74	94.13
VITAF* (Huang et al. 2022)	2.91	99.71	6.00	98.55	11.60	95.03
<b>G<sup>2</sup>V<sup>2</sup>former</b>	<b>2.59</b>	<b>99.20</b>	<b>4.99</b>	<b>98.62</b>	<b>9.58</b>	<b>95.60</b>

hope the temporal attention promptly focuses on more useful details. Facial landmarks can help identify the facial micro-motions that reveal differences between live and spoof motions, such as the motion in the corner of the mouth and eye blinking, which are all potential regions of interest. In Figure 4, each landmark belongs to a patch box, and the motion trajectory of landmarks can express facial motion to an extent. Thus, we naively believe patch boxes that contain landmarks are most likely to undergo pixel changes.

During fine-tuning, we utilize the sequence number of the patches as indexes where the landmark node is located. Nodes are scattered based on their patch sequence number indexes. After performing a scatter operation, the shape of the graph temporal attention matrix is aligned with the shape of the vision temporal attention matrix, and then adding them. In Figure 4, we provide an example demonstration with a patch number of 4 and a node number of 2. At  $t=0$ ,  $N_0$  belongs to the 0-th patch  $P_0$ ,  $N_1$  belongs to the 1-th patch  $P_1$ , while at  $t=1$ ,  $N_0$  belongs to the  $P_1$ , and  $N_1$  belongs to the  $P_3$ . In simpler terms, this involves replacing the row and column numbers of the graph temporal attention matrix with patch sequence numbers based on indexes. Subsequently, we select (scatter) and fill (add) elements. We term this operation scatter and add.

At each layer of the model, after executing the spatial attention of the graph and vision, we first calculate the graph

Table 3: Generalization evaluation on 3D mask attacks. Experiments are conducted on two popular 3D mask benchmarks, 3DMAD (denoted as 3DM) and HKBU-MARsV1 (denoted as HKM).

Method	O&C&I to 3DM		O&C&I to HKM	
	HTER(%)	AUC(%)	HTER(%)	AUC(%)
ResNet18 (He et al. 2016)	48.75	61.07	50.00	59.40
SSDG (Jia et al. 2020)	37.07	72.93	46.00	65.20
<b>G<sup>2</sup>V<sup>2</sup>former</b>	<b>1.26</b>	<b>99.69</b>	<b>9.34</b>	<b>95.52</b>

Kronecker temporal attention and cache its attention matrix. During the subsequent vision Kronecker temporal attention, the cached attention matrix is scattered and added as an attention bias, guiding the dynamic information capture for the vision stream:

$$B_{\text{guide}} = Q_{gt} K_{gt}^T / \sqrt{d_k}, \quad (15)$$

$$Z_{vt} = \text{Softmax}(Q_{vt} K_{vt}^T / \sqrt{d_k} + M + \text{ScatterAdd}(B_{\text{guide}})) V_{vt}, \quad (16)$$

where  $B_{\text{guide}}$  is graph guidance bias. The subscript  $gt$  represents the graph temporal attention, and  $vt$  represents the vision temporal attention.

## Experiment

### Datasets and Protocol

We use nine public datasets: Oulu-NPU (Boulkenafet et al. 2017) (denoted as O), CASIA-FASD (Zhang et al. 2012) (denoted as C), Idiap Replay-Attack (Chingovska, Anjos, and Marcel 2012) (denoted as I), MSU-MFSD (Wen, Han, and Jain 2015) (denoted as M), CASIA-SURF (Zhang et al. 2019, 2020), CASIA-CeFA (Liu et al. 2021b,a), WMCA (George et al. 2019), 3DMAD (Erdogmus and Marcel 2013), and HKBU-MARsV1 (Liu et al. 2016). We evaluate our model on the prevalent cross-dataset protocol to verify its effectiveness. To demonstrate the robust generalization capabilities of G<sup>2</sup>V<sup>2</sup>former, we assess its performance

Table 4: Ablation of each component on O&amp;C&amp;I to M.

Baseline	Landmarks	Graph guide	PCL	HTER(%)	AUC(%)
✓	-	-	-	5.03	97.69
✓	✓	-	-	4.91	97.94
✓	✓	✓	-	<b>3.88</b>	<b>99.01</b>
✓	✓	✓	✓	<b>3.72</b>	<b>99.24</b>

under the protocol of cross-dataset (3DM, HKM), cross-type (unseen attacks, 3D Mask). The evaluation metrics are Half Total Error Rate (HTER) and Area Under the Curve (AUC).

### Implementation Details

First, we extract all frames from each video and utilize the MTCNN (Zhang et al. 2016) for face detection, then crop and resize the images to  $224 \times 224$  for facial landmarks detection. We employ the 3DDFA-V2 (Guo et al. 2020) to obtain the 3-dimensional coordinates of landmarks. We apply random blurring, sharpening, 2D rotation, and affine transformation for data augmentation. It is worth noting that 2D rotation and affine transformation of image are also applied to landmarks. We set the patch size to 16, and the length of the input frames is 8. The sample interval depends on the total frames (default 8). When the total length is shorter, we try to reduce the sampling interval until the requirements are met. We use Adam optimizer (Kingma and Ba 2014), and the base learning rate is set to  $5e-4$  in pre-training,  $2e-4$  in fine-tuning. The scheduler for reducing learning rates is cosine decay (Loshchilov and Hutter 2016), and the total pre-training iterations are 60000, 20000 iterations for fine-tuning. The encoder and decoder adopt an asymmetric design, with 12 layers for the encoder and 4 layers for the decoder. Our method is implemented under the Pytorch framework. Please refer to the *supplementary materials* for more detailed experimental parameter settings and network architecture.

### Comparison with SOTA Methods

We evaluate our model under the Leave-One-Out (LOO) setting, which utilizes O, C, I, and M datasets. Besides, in order to demonstrate our model’s generalization of unseen attacks, we also used two additional datasets of 3D mask attacks for testing.

**Leave-One-Out (LOO).** In the LOO setting, we randomly select three datasets out of O, C, I, and M for training, while the remaining one is reserved for testing. These four datasets contain the same type of face samples (live, printed photo, video replay), but they encounter variations in capture device, illumination, resolution, etc. As depicted in Table 1, our method exhibits superior performance when compared with both frame-level methods and video-level methods (marked with a star). This reveals the significance of spatiotemporal fusion in face anti-spoofing tasks.

**Evaluation on CASIA-SURF, CASIA-CeFA and WMCA Protocol.** As shown in Table 2, we evaluate our method among CASIA-SURF, CASIA-CeFA and WMCA. They all exhibit rich and diverse variations of expression and motion. We follow the experimental setting in (Huang et al. 2022). Under the 0-shot and 5-shot scenarios, our  $G^2V^2$ former surpasses most previous methods. Due to our utilization of

Table 5: Comparison of different visual attention forms.

Attention Form	HTER (%)	AUC(%)
3D Convolution (wo-guide)	7.87	95.65
1D+2D Convolution (wo-guide)	7.90	96.21
Joint Spatial-Temporal (wo-guide)	6.33	96.86
Spatial-Temporal Pipeline (wo-guide)	6.06	96.74
<b>Spatial-Kronecker Temporal (wo-guide)</b>	<b>4.91</b>	<b>97.94</b>

both photometric and dynamic information, allow us to more fully mine spoofing cues.

**Generalization of Unseen Attacks.** The OCIM-LOO primarily consists of printed photos and video replay, focusing on the cross-dataset intra-type protocol which necessitates overcoming domain gaps. In contrast, the cross-dataset and cross-type protocols are more challenging. Defending 3D mask attacks, given their high degree of photorealism, demands specialized defense methods. However, defending against 3D mask attacks becomes challenging in the absence of relevant training samples. To explore the strengths of  $G^2V^2$ former in more demanding scenarios, we propose two cross-dataset cross-type protocols: O&C&I to 3DM, and O&C&I to HKM. The 3DM (3DMAD (Erdogmus and Marcel 2013)), and HKM (HKBU-MARsV1 (Liu et al. 2016)) involve low, high-photorealism custom wearable masks. For comparison, we select a representative photometric-based algorithm SSDG (Jia et al. 2020) and vanilla ResNet18 (He et al. 2016). As depicted in Table 3, SSDG experienced a significant performance drop, ResNet18 is vulnerable or even ineffective, while our method still holds on. This indicates that the  $G^2V^2$ former has an unexpected generalization ability. The performance on HKBU-MARsV1 is slightly inferior because its 3D mask has higher photorealism.

### Ablation Studies

In this subsection, we conduct ablation studies to explore the efforts of each component. We also compare various spatiotemporal modules for spatiotemporal fusion with our spatial & Kronecker temporal attention module. The results indicate that our Kronecker temporal attention is more suitable for FAS tasks. It should be noted that both the ablation study and comparison experiments are conducted under O&C&I& to M settings.

**Contribution of Different Components.** Table 4 shows the ablation studies. For the baseline configuration, we employ the TimeSformer (Bertasius, Wang, and Torresani 2021) as the backbone equipped with spatial & Kronecker temporal attention and extract the class token for classification. Then we introduce the graph stream whose input is facial landmarks. In this case, we naively concatenate the class token and hyper-node token for classification. Besides, we attempted to use the lower semantic coordinate motion of landmarks to guide vision temporal attention to capture higher semantic pixel motion over time. Finally, Photometric consistency loss is added to highlight the photometric characteristic in spatial attention. We can observe that under our baseline configuration, the performance has reached a relatively high value. After introducing landmarks without guidance, the performance has an improvement. When further exploring the exploitable value of the landmark, i.e.,

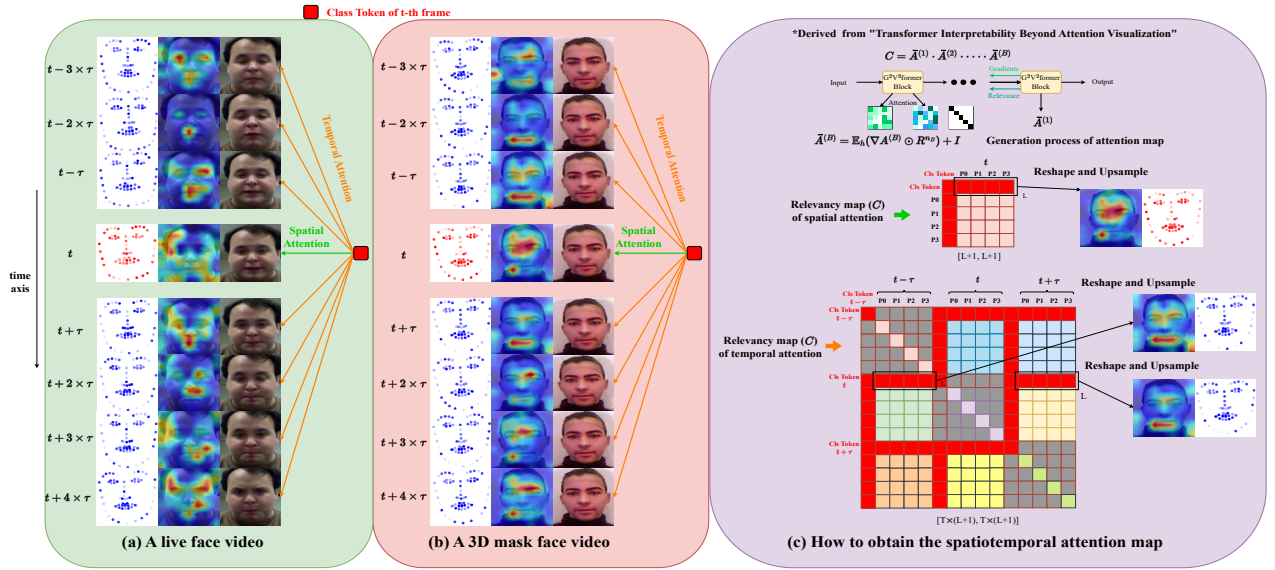


Figure 5: (a) and (b) Utilizing Transformer Explainability (Chefer, Gur, and Wolf 2021) to visualize a comprehensive spatiotemporal attention map. For vision branch, the transition from warm to cool colors corresponding to a shift from interested to uninterested. While in graph branch, the transition from opacity to transparency mirrors a change in attention values from high to low. (c) How to obtain the spatiotemporal attention map.

mining the high-level pixel motion semantic, points further increase. When introduce photometric consistency loss, our model reaches a peak in performance.

**Comparison of Different Spatiotemporal Modules.** Table 5 depicts the comparison of different spatiotemporal modules. For the sake of fairness, we compared them without graphic guidance, due to the graphic guidance is incompatible with some of them. The results indicate that our method has advantages compared to the other spatiotemporal fusion module to the extent, and the Kronecker temporal attention is more beneficial for FAS tasks where pixel motion is not obvious.

## Visualization and Analysis

**Spatiotemporal Attention Visualization.** We sample 8 frames of live faces and 3D masks to illustrate the attention map. In Figure 5, the spatial attention reveals which regions of the  $t$ -th frame are highlighted, while the temporal attention shows which regions of other frames (except for  $t$ -th frame) receive more focus. In spatial attention, we observe that the red response area corresponds to the several facial area and background, responsible for capturing photometric information, potentially related to materials, textures, or lighting. However, temporal attention is more concentrated on motion areas, such as the mouth’s motion in live videos, or the awareness of the absence of variations of facial expressions in spoof videos. We utilize the Transformer Explainability (Chefer, Gur, and Wolf 2021) to present the visualization and provide a brief description of the process of generating attention maps. For each attention layer, we can obtain the attention map  $A^{(b)}$  and its gradients  $\nabla A^{(b)}$ , and relevance  $R^{n_b}$ , where  $n_b$  is the layer that corresponds to the Softmax operation in Equation 17 of transformer block  $b$ ,

and  $R^{n_b}$  is the layer’s relevance. Following the propagation rule of relevance and gradient illustrated on the upper right of Figure 5, we can conclude the final relevancy maps in Equation 19,20:

$$A^{(b)} = \text{Softmax}(Q^{(b)}K^{(b)T}/\sqrt{d_k}), \quad (17)$$

$$O^{(b)} = A^{(b)}V^{(b)}, \quad (18)$$

$$\bar{A}^{(b)} = I + \mathbb{E}_h(\nabla A^{(b)} \odot R^{n_b})+, \quad (19)$$

$$C = \bar{A}^{(1)} \cdot \bar{A}^{(2)} \cdot \dots \cdot \bar{A}^{(B)}, \quad (20)$$

where  $\odot$  is the Hadamard product, and  $\mathbb{E}_h$  is the mean across the “heads” dimension.  $C$  is the final output for visualization.

For the spatial attention’s relevancy map of  $t$ -th frame, its shape is  $[L+1, L+1]$ . We take the attention weight corresponding to the first row except for the class token itself, with a length of  $L$ , where  $L$  is the number of patches, and reshape it into 2D. By upsampling, we can obtain the spatial attention map. While the shape of temporal attention’s relevancy map is  $[T \times (L+1), T \times (L+1)]$ , where  $T$  is the number of frames. We take the time segment from  $t-\tau$  to  $t+\tau$  as an example, because masking of the same frame patch by our Kronecker temporal attention, we only need to take attention weights in different timestamps. Two weight sequences with a length of  $L$  correspond to the temporal attention map of frame  $t$  regarding  $t-\tau$  and  $t+\tau$ . We use the same method to obtain graph attention maps. In terms of time dimension, the model is more interested in the mouth, eyes, and eyebrow bones because these areas have a higher probability of relative movement. In spatial attention, the areas of interest are relatively scattered, dedicated to perceiving the topology of facial landmarks. For more visualization and analysis, please refer to the *supplementary materials*.

## Conclusion

This study introduces a pioneering architecture Graph Guided Video Vision Transformer ( $G^2V^2$ former) to capture discriminative spatiotemporal spoofing shreds of evidence for the FAS task by concurrently leveraging facial images and landmarks. We factorize the joint attention into spatial and temporal attention, utilizing photometric consistency loss to guide the spatial attention. We propose a novel Kronecker temporal attention with wider receptive field, and then utilize the motion trajectory contained in facial landmarks to guide the pixel motion capture. Through extensive experiments and ablation studies, we demonstrate the effectiveness of  $G^2V^2$ former which achieves extraordinary generalization even in more challenging scenarios.

## References

- Arnab, A.; Deghani, M.; Heigold, G.; Sun, C.; Lučić, M.; and Schmid, C. 2021. Vivit: A video vision transformer. In *Proceedings of the IEEE/CVF international conference on computer vision*, 6836–6846.
- Bertasius, G.; Wang, H.; and Torresani, L. 2021. Is space-time attention all you need for video understanding? In *ICML*, volume 2, 4.
- Boulkenafet, Z.; Komulainen, J.; and Hadid, A. 2015. Face anti-spoofing based on color texture analysis. In *2015 IEEE international conference on image processing (ICIP)*, 2636–2640. IEEE.
- Boulkenafet, Z.; Komulainen, J.; Li, L.; Feng, X.; and Hadid, A. 2017. OULU-NPU: A mobile face presentation attack database with real-world variations. In *2017 12th IEEE international conference on automatic face & gesture recognition (FG 2017)*, 612–618. IEEE.
- Chang, C.-J.; Lee, Y.-C.; Yao, S.-H.; Chen, M.-H.; Wang, C.-Y.; Lai, S.-H.; and Chen, T. P.-C. 2023. A Closer Look at Geometric Temporal Dynamics for Face Anti-Spoofing. In *Proceedings of the IEEE/CVF Conference on Computer Vision and Pattern Recognition Biometrics Workshop*, 1081–1091.
- Chefer, H.; Gur, S.; and Wolf, L. 2021. Transformer interpretability beyond attention visualization. In *Proceedings of the IEEE/CVF conference on computer vision and pattern recognition*, 782–791.
- Chen, Z.; Yao, T.; Sheng, K.; Ding, S.; Tai, Y.; Li, J.; Huang, F.; and Jin, X. 2021. Generalizable representation learning for mixture domain face anti-spoofing. In *Proceedings of the AAAI Conference on Artificial Intelligence*, volume 35, 1132–1139.
- Chingovska, I.; Anjos, A.; and Marcel, S. 2012. On the effectiveness of local binary patterns in face anti-spoofing. In *2012 BIOSIG-proceedings of the international conference of biometrics special interest group (BIOSIG)*, 1–7. IEEE.
- Dosovitskiy, A.; Beyer, L.; Kolesnikov, A.; Weissenborn, D.; Zhai, X.; Unterthiner, T.; Deghani, M.; Minderer, M.; Heigold, G.; Gelly, S.; et al. 2020. An image is worth 16x16 words: Transformers for image recognition at scale. *arXiv preprint arXiv:2010.11929*.
- Erdogmus, N.; and Marcel, S. 2013. Spoofing in 2d face recognition with 3d masks and anti-spoofing with kinect. In *2013 IEEE sixth international conference on biometrics: theory, applications and systems (BTAS)*, 1–6. IEEE.
- Feichtenhofer, C.; Li, Y.; He, K.; et al. 2022. Masked autoencoders as spatiotemporal learners. *Advances in neural information processing systems*, 35: 35946–35958.
- George, A.; Mostaani, Z.; Geissenbuhler, D.; Nikisins, O.; Anjos, A.; and Marcel, S. 2019. Biometric face presentation attack detection with multi-channel convolutional neural network. *IEEE transactions on information forensics and security*, 15: 42–55.
- Guo, J.; Zhu, X.; Yang, Y.; Yang, F.; Lei, Z.; and Li, S. Z. 2020. Towards fast, accurate and stable 3d dense face alignment. In *European Conference on Computer Vision*, 152–168. Springer.
- Guo, X.; Guo, X.; and Lu, Y. 2021. Ssan: Separable self-attention network for video representation learning. In *Proceedings of the IEEE/CVF conference on computer vision and pattern recognition*, 12618–12627.
- He, K.; Chen, X.; Xie, S.; Li, Y.; Dollár, P.; and Girshick, R. 2022. Masked autoencoders are scalable vision learners. In *Proceedings of the IEEE/CVF conference on computer vision and pattern recognition*, 16000–16009.
- He, K.; Zhang, X.; Ren, S.; and Sun, J. 2016. Deep residual learning for image recognition. In *Proceedings of the IEEE conference on computer vision and pattern recognition*, 770–778.
- Huang, H.-P.; Sun, D.; Liu, Y.; Chu, W.-S.; Xiao, T.; Yuan, J.; Adam, H.; and Yang, M.-H. 2022. Adaptive transformers for robust few-shot cross-domain face anti-spoofing. In *European conference on computer vision*, 37–54. Springer.
- Jia, Y.; Zhang, J.; Shan, S.; and Chen, X. 2020. Single-side domain generalization for face anti-spoofing. In *Proceedings of the IEEE/CVF Conference on Computer Vision and Pattern Recognition*, 8484–8493.
- Khan, S. A.; and Dai, H. 2021. Video transformer for deepfake detection with incremental learning. In *Proceedings of the 29th ACM International Conference on Multimedia*, 1821–1828.
- Kingma, D. P.; and Ba, J. 2014. Adam: A method for stochastic optimization. *arXiv preprint arXiv:1412.6980*.
- Kollreider, K.; Fronthaler, H.; Faraj, M. I.; and Bigun, J. 2007. Real-time face detection and motion analysis with application in “liveness” assessment. *IEEE Transactions on Information Forensics and Security*, 2(3): 548–558.
- Le, B. M.; and Woo, S. S. 2024. Gradient alignment for cross-domain face anti-spoofing. In *Proceedings of the IEEE/CVF Conference on Computer Vision and Pattern Recognition*, 188–199.
- Li, H.; Pan, S. J.; Wang, S.; and Kot, A. C. 2018. Domain generalization with adversarial feature learning. In *Proceedings of the IEEE conference on computer vision and pattern recognition*, 5400–5409.
- Li, L.; Feng, X.; Boulkenafet, Z.; Xia, Z.; Li, M.; and Hadid, A. 2016a. An original face anti-spoofing approach using



- partial convolutional neural network. In *2016 Sixth International Conference on Image Processing Theory, Tools and Applications (IPTA)*, 1–6. IEEE.
- Li, X.; Komulainen, J.; Zhao, G.; Yuen, P.-C.; and Pietikäinen, M. 2016b. Generalized face anti-spoofing by detecting pulse from face videos. In *2016 23rd International Conference on Pattern Recognition (ICPR)*, 4244–4249. IEEE.
- Liu, A.; Li, X.; Wan, J.; Liang, Y.; Escalera, S.; Escalante, H. J.; Madadi, M.; Jin, Y.; Wu, Z.; Yu, X.; et al. 2021a. Cross-ethnicity face anti-spoofing recognition challenge: A review. *IET Biometrics*, 10(1): 24–43.
- Liu, A.; Tan, Z.; Wan, J.; Escalera, S.; Guo, G.; and Li, S. Z. 2021b. Casia-surf cefa: A benchmark for multi-modal cross-ethnicity face anti-spoofing. In *Proceedings of the IEEE/CVF winter conference on applications of computer vision*, 1179–1187.
- Liu, S.; Yuen, P. C.; Zhang, S.; and Zhao, G. 2016. 3D mask face anti-spoofing with remote photoplethysmography. In *Computer Vision—ECCV 2016: 14th European Conference, Amsterdam, The Netherlands, October 11–14, 2016, Proceedings, Part VII 14*, 85–100. Springer.
- Liu, S.; Zhang, K.-Y.; Yao, T.; Bi, M.; Ding, S.; Li, J.; Huang, F.; and Ma, L. 2021c. Adaptive normalized representation learning for generalizable face anti-spoofing. In *Proceedings of the 29th ACM international conference on multimedia*, 1469–1477.
- Liu, S.; Zhang, K.-Y.; Yao, T.; Sheng, K.; Ding, S.; Tai, Y.; Li, J.; Xie, Y.; and Ma, L. 2021d. Dual reweighting domain generalization for face presentation attack detection. *arXiv preprint arXiv:2106.16128*.
- Liu, S.-Q.; Lan, X.; and Yuen, P. C. 2018. Remote photoplethysmography correspondence feature for 3D mask face presentation attack detection. In *Proceedings of the European Conference on Computer Vision (ECCV)*, 558–573.
- Liu, Y.; Chen, Y.; Gou, M.; Huang, C.-T.; Wang, Y.; Dai, W.; and Xiong, H. 2023. Towards unsupervised domain generalization for face anti-spoofing. In *Proceedings of the IEEE/CVF International Conference on Computer Vision*, 20654–20664.
- Liu, Y.; Jourabloo, A.; and Liu, X. 2018. Learning deep models for face anti-spoofing: Binary or auxiliary supervision. In *Proceedings of the IEEE conference on computer vision and pattern recognition*, 389–398.
- Liu, Z.; Lin, Y.; Cao, Y.; Hu, H.; Wei, Y.; Zhang, Z.; Lin, S.; and Guo, B. 2021e. Swin transformer: Hierarchical vision transformer using shifted windows. In *Proceedings of the IEEE/CVF international conference on computer vision*, 10012–10022.
- Liu, Z.; Ning, J.; Cao, Y.; Wei, Y.; Zhang, Z.; Lin, S.; and Hu, H. 2022. Video swin transformer. In *Proceedings of the IEEE/CVF conference on computer vision and pattern recognition*, 3202–3211.
- Loshchilov, I.; and Hutter, F. 2016. Sgdr: Stochastic gradient descent with warm restarts. *arXiv preprint arXiv:1608.03983*.
- Mildenhall, B.; Srinivasan, P. P.; Tancik, M.; Barron, J. T.; Ramamoorthi, R.; and Ng, R. 2021. Nerf: Representing scenes as neural radiance fields for view synthesis. *Communications of the ACM*, 65(1): 99–106.
- Ming, Z.; Yu, Z.; Al-Ghadi, M.; Visani, M.; Luqman, M. M.; and Burie, J.-C. 2022. Vitranspad: video transformer using convolution and self-attention for face presentation attack detection. In *2022 IEEE International Conference on Image Processing (ICIP)*, 4248–4252. IEEE.
- Neimark, D.; Bar, O.; Zohar, M.; and Asselmann, D. 2021. Video transformer network. In *Proceedings of the IEEE/CVF international conference on computer vision*, 3163–3172.
- Patel, K.; Han, H.; and Jain, A. K. 2016a. Cross-database face antispoofing with robust feature representation. In *Biometric Recognition: 11th Chinese Conference, CCBR 2016, Chengdu, China, October 14-16, 2016, Proceedings 11*, 611–619. Springer.
- Patel, K.; Han, H.; and Jain, A. K. 2016b. Secure face unlock: Spoof detection on smartphones. *IEEE transactions on information forensics and security*, 11(10): 2268–2283.
- Saha, S.; Xu, W.; Kanakis, M.; Georgoulis, S.; Chen, Y.; Paudel, D. P.; and Van Gool, L. 2020. Domain agnostic feature learning for image and video based face anti-spoofing. In *Proceedings of the IEEE/CVF Conference on Computer Vision and Pattern Recognition Workshops*, 802–803.
- Shao, R.; Lan, X.; Li, J.; and Yuen, P. C. 2019. Multi-adversarial discriminative deep domain generalization for face presentation attack detection. In *Proceedings of the IEEE/CVF conference on computer vision and pattern recognition*, 10023–10031.
- Shao, R.; Lan, X.; and Yuen, P. C. 2017. Deep convolutional dynamic texture learning with adaptive channel-discriminability for 3D mask face anti-spoofing. In *2017 IEEE International Joint Conference on Biometrics (IJCB)*, 748–755. IEEE.
- Shao, R.; Lan, X.; and Yuen, P. C. 2020. Regularized fine-grained meta face anti-spoofing. In *Proceedings of the AAAI Conference on Artificial Intelligence*, volume 34, 11974–11981.
- Sun, Y.; Liu, Y.; Liu, X.; Li, Y.; and Chu, W.-S. 2023. Rethinking Domain Generalization for Face Anti-spoofing: Separability and Alignment. In *Proceedings of the IEEE/CVF Conference on Computer Vision and Pattern Recognition*, 24563–24574.
- Tong, Z.; Song, Y.; Wang, J.; and Wang, L. 2022. Video-mae: Masked autoencoders are data-efficient learners for self-supervised video pre-training. *Advances in neural information processing systems*, 35: 10078–10093.
- Wang, C.-Y.; Lu, Y.-D.; Yang, S.-T.; and Lai, S.-H. 2022a. Patchnet: A simple face anti-spoofing framework via fine-grained patch recognition. In *Proceedings of the IEEE/CVF Conference on Computer Vision and Pattern Recognition*, 20281–20290.
- Wang, G.; Han, H.; Shan, S.; and Chen, X. 2020a. Unsupervised adversarial domain adaptation for cross-domain face

- presentation attack detection. *IEEE Transactions on Information Forensics and Security*, 16: 56–69.
- Wang, J.; Zhang, J.; Bian, Y.; Cai, Y.; Wang, C.; and Pu, S. 2021a. Self-domain adaptation for face anti-spoofing. In *Proceedings of the AAAI Conference on Artificial Intelligence*, volume 35, 2746–2754.
- Wang, Z.; Wang, Q.; Deng, W.; and Guo, G. 2022b. Learning multi-granularity temporal characteristics for face anti-spoofing. *IEEE Transactions on Information Forensics and Security*, 17: 1254–1269.
- Wang, Z.; Wang, Z.; Yu, Z.; Deng, W.; Li, J.; Gao, T.; and Wang, Z. 2022c. Domain generalization via shuffled style assembly for face anti-spoofing. In *Proceedings of the IEEE/CVF Conference on Computer Vision and Pattern Recognition*, 4123–4133.
- Wang, Z.; Xu, Y.; Wu, L.; Han, H.; Ma, Y.; and Ma, G. 2021b. Multi-perspective features learning for face anti-spoofing. In *Proceedings of the IEEE/CVF International Conference on Computer Vision*, 4116–4122.
- Wang, Z.; Yu, Z.; Zhao, C.; Zhu, X.; Qin, Y.; Zhou, Q.; Zhou, F.; and Lei, Z. 2020b. Deep spatial gradient and temporal depth learning for face anti-spoofing. In *Proceedings of the IEEE/CVF Conference on Computer Vision and Pattern Recognition*, 5042–5051.
- Wen, D.; Han, H.; and Jain, A. K. 2015. Face spoof detection with image distortion analysis. *IEEE Transactions on Information Forensics and Security*, 10(4): 746–761.
- Xu, Y.; Wang, Z.; Han, H.; Wu, L.; and Liu, Y. 2021. Exploiting non-uniform inherent cues to improve presentation attack detection. In *2021 IEEE International Joint Conference on Biometrics (IJCB)*, 1–8. IEEE.
- Yan, S.; Xiong, Y.; and Lin, D. 2018. Spatial temporal graph convolutional networks for skeleton-based action recognition. In *Proceedings of the AAAI conference on artificial intelligence*, volume 32.
- Yang, J.; Lei, Z.; Liao, S.; and Li, S. Z. 2013. Face liveness detection with component dependent descriptor. In *2013 International Conference on Biometrics (ICB)*, 1–6. IEEE.
- Yang, J.; Yu, Z.; Ni, X.; He, J.; and Li, H. 2024. Generalized Face Anti-spoofing via Finer Domain Partition and Disentangling Liveness-irrelevant Factors. *European Conference on Artificial Intelligence (ECAI)*.
- Yang, X.; Luo, W.; Bao, L.; Gao, Y.; Gong, D.; Zheng, S.; Li, Z.; and Liu, W. 2019. Face anti-spoofing: Model matters, so does data. In *Proceedings of the IEEE/CVF Conference on Computer Vision and Pattern Recognition*, 3507–3516.
- Ying, C.; Cai, T.; Luo, S.; Zheng, S.; Ke, G.; He, D.; Shen, Y.; and Liu, T.-Y. 2021. Do transformers really perform badly for graph representation? *Advances in Neural Information Processing Systems*, 34: 28877–28888.
- Yu, Z.; Li, X.; Wang, P.; and Zhao, G. 2021. Transrppg: Remote photoplethysmography transformer for 3d mask face presentation attack detection. *IEEE Signal Processing Letters*, 28: 1290–1294.
- Yu, Z.; Wan, J.; Qin, Y.; Li, X.; Li, S. Z.; and Zhao, G. 2020a. NAS-FAS: Static-dynamic central difference network search for face anti-spoofing. *IEEE transactions on pattern analysis and machine intelligence*, 43(9): 3005–3023.
- Yu, Z.; Zhao, C.; Wang, Z.; Qin, Y.; Su, Z.; Li, X.; Zhou, F.; and Zhao, G. 2020b. Searching central difference convolutional networks for face anti-spoofing. In *Proceedings of the IEEE/CVF Conference on Computer Vision and Pattern Recognition*, 5295–5305.
- Zhang, K.; Zhang, Z.; Li, Z.; and Qiao, Y. 2016. Joint face detection and alignment using multitask cascaded convolutional networks. *IEEE signal processing letters*, 23(10): 1499–1503.
- Zhang, S.; Liu, A.; Wan, J.; Liang, Y.; Guo, G.; Escalera, S.; Escalante, H. J.; and Li, S. Z. 2020. Casia-surf: A large-scale multi-modal benchmark for face anti-spoofing. *IEEE Transactions on Biometrics, Behavior, and Identity Science*, 2(2): 182–193.
- Zhang, S.; Wang, X.; Liu, A.; Zhao, C.; Wan, J.; Escalera, S.; Shi, H.; Wang, Z.; and Li, S. Z. 2019. A dataset and benchmark for large-scale multi-modal face anti-spoofing. In *Proceedings of the IEEE/CVF Conference on Computer Vision and Pattern Recognition*, 919–928.
- Zhang, Z.; Yan, J.; Liu, S.; Lei, Z.; Yi, D.; and Li, S. Z. 2012. A face antispoofing database with diverse attacks. In *2012 5th IAPR international conference on Biometrics (ICB)*, 26–31. IEEE.
- Zhou, Q.; Zhang, K.-Y.; Yao, T.; Lu, X.; Ding, S.; and Ma, L. 2024. Test-time domain generalization for face anti-spoofing. In *Proceedings of the IEEE/CVF Conference on Computer Vision and Pattern Recognition*, 175–187.
- Zhou, Q.; Zhang, K.-Y.; Yao, T.; Lu, X.; Yi, R.; Ding, S.; and Ma, L. 2023. Instance-Aware Domain Generalization for Face Anti-Spoofing. In *Proceedings of the IEEE/CVF Conference on Computer Vision and Pattern Recognition*, 20453–20463.